

AN EMERGING TECHNOLOGY FOR FUSION: THE SPHERICAL PINCH

E. Panarella*

Department of Electrical and Computer Engineering
University of Tennessee
Knoxville, TN 37996-2100, U.S.A.

ABSTRACT

Several years of research and development in a particular plasma configuration designated by the name of Spherical Pinch has led to a device that provides short-term industrial benefits and long-term nuclear fusion energy benefits. The former benefits derive from its exploitation as a soft X-ray generator for microlithography and as a neutron generator for nondestructive detection of hidden defects and corrosion in metallic structures. The latter benefits derive from its potential to approach fusion breakeven conditions in a spherical configuration which is essentially a modification of the well known inertial confinement fusion configuration. This paper highlights the milestones of the research program on the Spherical Pinch carried out in the past several years, up to the present status of the Spherical Pinch concept both as a nuclear fusion device and an industrial tool.

INTRODUCTION

Since the late 70s an experimental and theoretical program has been carried out at the National Research Council of Canada in Ottawa on an evolution of a well-known plasma physics concept, the theta pinch, from the cylindrical geometry to the spherical. The motivation for such a study was given by the ability of the spherical configuration to overcome the serious problem of plasma end losses inherent in the cylindrical geometry. If this scheme was supplemented by the presence of a hot plasma in the centre of the spherical vessel, which would act as a target for the imploding shock waves generated in the spherical pinch, these would then compress such central plasma, contain it, and further raise its temperature. The spherical pinch concept could then lead to a machine capable of seriously competing in the fusion race.

The conversion from cylindrical to spherical geometry along the lines indicated above was successful. A number of experiments were carried out and copious X-ray and neutron emission was observed from modest scale plasmas.⁽¹⁾ This, in turn, led at the beginning of the 80s to analyze in depth the experimental conditions required for a spherical pinch to satisfy the Lawson

*Also with Advanced Laser and Fusion Technology, Inc.
189 Deveault St., #7, Hull, P.Q., J8Z 1S7, Canada

criteria for breakeven fusion conditions. Following an intensive study and modelling of the phenomenon, in 1983 the scaling laws for spherical pinch devices were derived.⁽²⁾ Although obtained under simplifying conditions, they nevertheless indicated that the spherical pinch concept had the potential of reaching breakeven fusion conditions. A series of pilot experiments designed to approach the conditions required by the scaling laws were then carried out, which verified the stability of the spherically pinched plasma under those conditions, and neutron emission, a signature of fusion reactions, was again observed.^(3,4)

Encouraged by these successes, industrial interest in the Spherical Pinch has recently been manifested. In 1987 a Company (Advanced Laser and Fusion Technology, Inc. - ALFT) became operational in Canada and a particular target industrial spinoff, soft X-ray production for microlithography^(5,6), was selected as initial application of the Spherical Pinch. This project has now completed the stage of final machine prototyping, and the production and marketing stages are beginning.

Another industrial spinoff of the Spherical Pinch is now being seriously considered. It is neutron generation for nondestructive testing of materials. A Feasibility Study has been recently concluded which indicates that the Spherical Pinch can become a transportable neutron generator for a neutron radiography system. An experimental proof-of-principle stage is now being planned, in which a 1 MJ condenser bank facility will be used for the project.

The knowledge acquired through these industrial spinoffs on the basic operation and characteristics of the Spherical Pinch has proven fundamental in understanding the direction to follow to reach fusion ignition conditions with this machine. In particular, a recent numerical study carried out with realistic energy input parameters has revealed that the Spherical Pinch can become a serious contender for fusion⁽⁷⁾. The advantages of pursuing this line of research are therefore: 1) the laws that govern the phenomenon are known and understood; 2) experiments aimed at proving conditions near or at ignition are, by all standards, modest scale experiments, and therefore economical; and 3) even if ignition conditions are not achieved in the short term, the Spherical Pinch is already providing economical returns through its industrial spinoffs.

In the following sections a broad overview of past achievements in the Spherical Pinch program will be provided, and future directions of research will be outlined.

LAWSON CRITERION FOR BREAKEVEN FUSION CONDITIONS

For a successful thermonuclear reactor working with a mixture of deuterium and tritium the following two conditions have to be satisfied⁽⁸⁾:

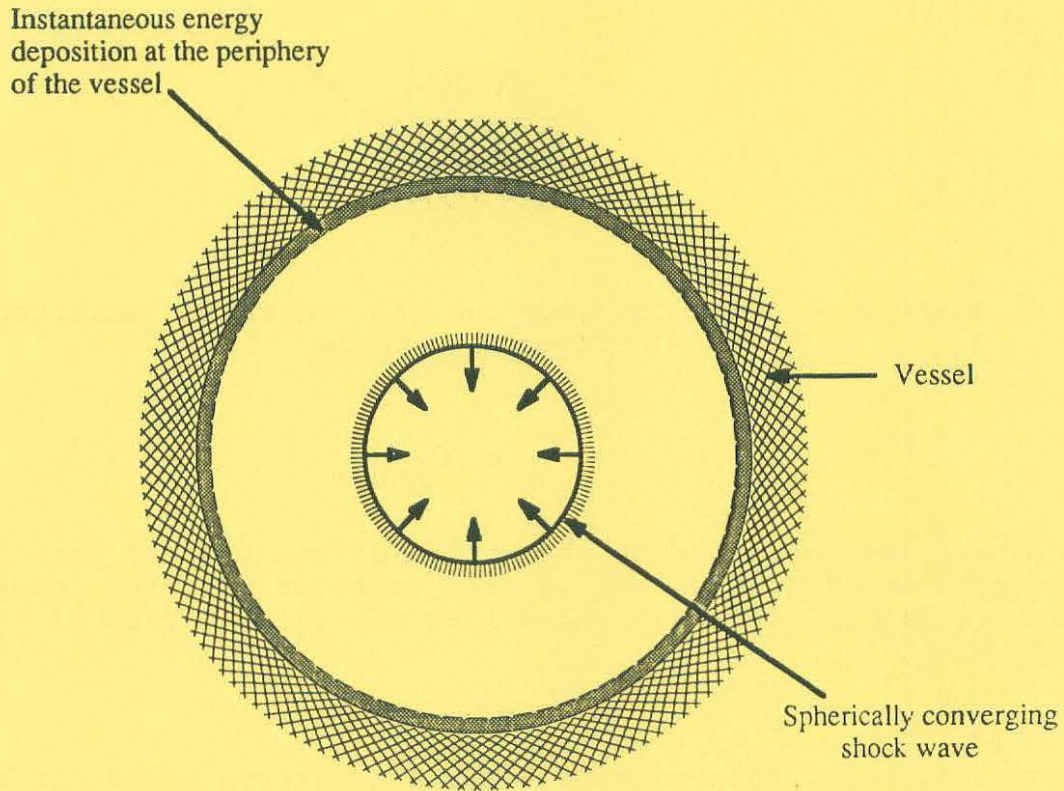


Fig. 1 - Inertial confinement fusion scheme

1. Critical temperature: $T \geq 2.58 \text{ keV}$ (for $nt_c \rightarrow \infty$).
2. Particle number density n x plasma containment time t_c : $nt_c \geq 10^{14} \text{ cm}^{-3} \cdot \text{sec}$.

It is towards the attainment of these conditions that all fusion devices address their effort. Since the Spherical Pinch is essentially a modified Inertial Confinement Fusion scheme, in the following sections we will briefly outline the fundamental features of the latter scheme, and contrast it with the former.

INERTIAL CONFINEMENT FUSION

This scheme relies on the sudden deposition of a large amount of energy at the periphery of a spherical vessel in order to generate strong imploding shock waves that converge towards the centre. (Fig. 1). The most significant characteristic of this scheme is the pressure amplification behind the shock front due to shock area convergence effects. Theoretically, the shock pressure amplification varies proportionally to the inverse of the radius of the shock front⁽⁹⁾:

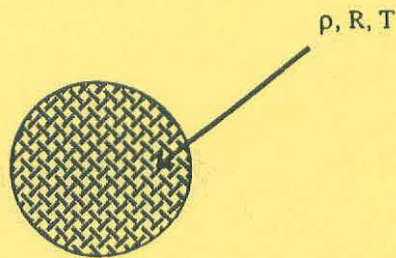


Fig. 2 - Final plasma in the inertial confinement fusion scheme

$$p \propto \frac{1}{R^{0.907}} \quad (1)$$

At shock collapse time at the centre of the vessel, this large pressure amplification can be used to raise the final plasma temperature to very high values, as the gas equation of state indicates:

$$p = nkT. \quad (2)$$

Temperatures of the order of 8 KeV and neutron yields of about 10^{10} have been obtained with this scheme⁽¹⁰⁾. However, the final particle number density required to satisfy the second Lawson criterion for breakeven is difficult to attain because the density behind the shock front can at most increase by a factor of ~ 4 , as the following formula of shock wave theory demonstrates:

$$\frac{\rho_1}{\rho_2} = \frac{\gamma + 1}{\gamma - 1} \approx 4 \quad (3)$$

where ρ_1 is the gas density behind the shock front, ρ_2 is the gas density in front of it, and $\gamma = \frac{5}{3}$ is the adiabatic index. In other words, the density does not increase indefinitely and, therefore, the main limitation of this scheme is the particle density that cannot reach the value required for breakeven conditions. The effect of this limitation will be seen more clearly in the next section.

SCALING LAW FOR INERTIAL CONFINEMENT FUSION

In the Inertial Confinement Fusion scheme, after the shock wave collapses at the centre of the vessel, the final "blob" of plasma does not persist in a hot state and rapidly expands by reflection (Fig. 2). The "confinement time" t_c is proportional to the time taken for a rarefaction wave to cross the plasma. In order to take into account the reduction in reaction rate as the density falls, we put

$$t_c = \frac{1}{2} \frac{R}{c_s} \quad (4)$$

where c_s is the sound speed at temperature T . Sequentially, one has:

$$n t_c \geq 10^{14} \text{ cm}^{-3} \cdot \text{sec}$$

$$\frac{r}{m_H} \frac{1}{2} \frac{R}{c_s} \geq 10^{14} \text{ cm}^{-3} \cdot \text{sec}$$

where we have replaced for n the value $\frac{\rho}{m_H}$, and for t_c the value provided by (4). One has:

$$\begin{aligned} \rho R &\geq 2 \times 10^{14} m_H \cdot c_s && \text{g.cm}^{-2} \\ \rho R &\geq 3 \text{ g.cm}^{-2} && (5) \end{aligned}$$

where ρ is the final density, R is the radius of that plasma which is hot enough to provide a significant number of nuclear reactions, and m_H is the proton mass. One derives:

$$\rho = 200 \text{ g.cm}^{-3} \quad (= 1000 \times \text{its normal density}) \quad (6)$$

Compression to this density is required for efficient thermonuclear burn. This is a very high density.

FURTHER CONSIDERATIONS ON THE INERTIAL CONFINEMENT FUSION MODEL

Because the deposition of energy at the periphery of the vessel is obtained with either laser beams, ion beams, or electron beams, this entails two main drawbacks:

- large and expensive machines are necessary;
- the overall efficiency of the system is rather poor ($< 1\%$), because electrical energy must be converted first into optical, ion, or electron energy, and then into plasma energy.

Moreover, the final plasma parameters, and in particular the ρR product, cannot easily be obtained.

THE SPHERICAL PINCH MODEL

In the Spherical Pinch, the large pressure amplification due to shock area convergence effect is now used to act upon a preformed

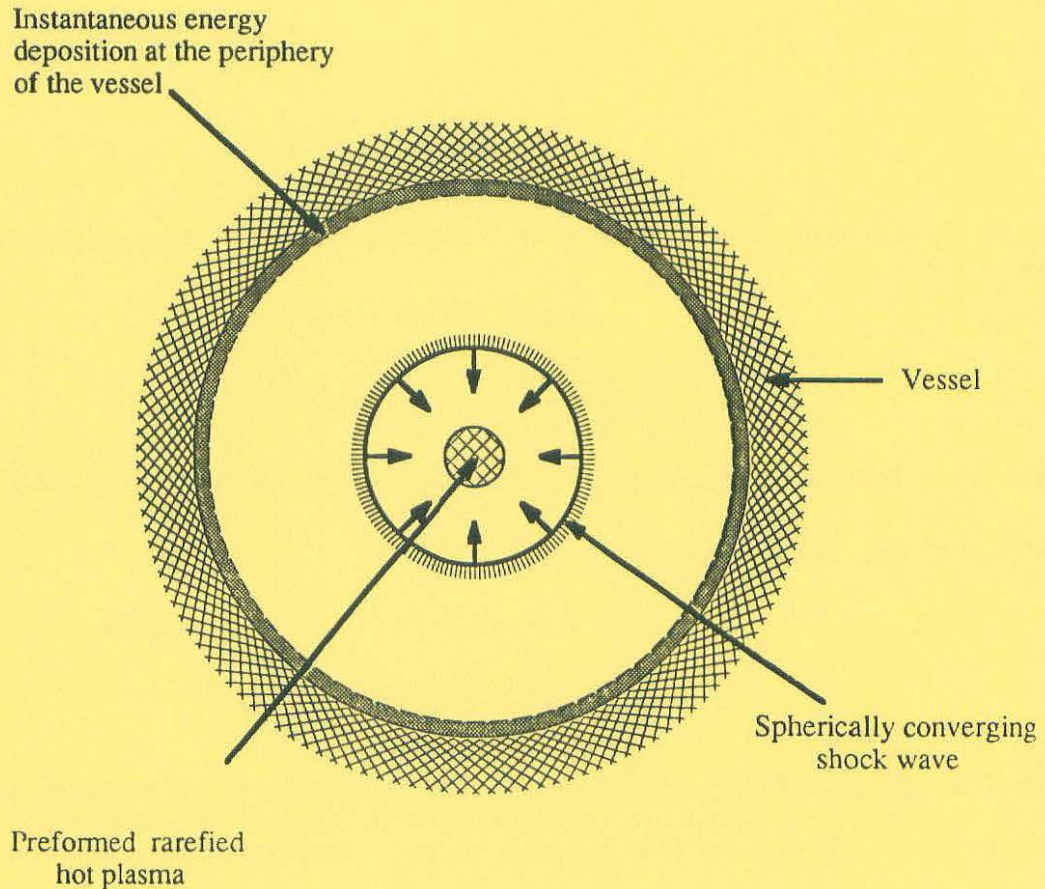


Fig. 3 - Spherical Pinch scheme

rarefied hot plasma, which is compressed by the imploding shock waves, thus raising further its temperature (Fig.3). The containment time can now be adjusted according to a well defined scaling law for breakeven fusion conditions, as we shall see in the following sections.

COMPARISON OF THE TWO SCHEMES

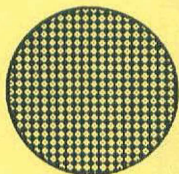
From the above illustrations of the two concepts, we see that they differ in the sense that the Inertial Confinement Fusion deals with very high density plasmas and very short confinement times, whereas the Spherical Pinch deals with relatively low density plasmas and long confinement times (Fig. 4).

OTHER FAVOURABLE FEATURES OF THE SPHERICAL PINCH

There are other features that make the Spherical Pinch attractive relative to the Inertial Confinement scheme. They are:

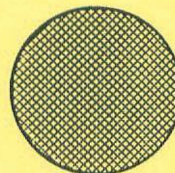
1. In the Spherical Pinch, the energy from a condenser bank goes directly into creating a plasma at the periphery of the

INERTIAL CONFINEMENT
FUSION



- very high density
- very short confinement time

SPHERICAL PINCH



- low density
- long confinement time

Fig. 4 - Comparison of the Inertial Confinement with the Spherical Pinch fusion scheme

spherical vessel; therefore, a transfer efficiency from electrical into plasma energy of up to 30% can be reached in this way;

2. Better control of the final plasma parameters, such as density, temperature and containment times are achieved, as the scaling law enunciated in the following sections will demonstrate.

SCHEMATIC SEQUENCE OF SPHERICAL PINCH OPERATIONS

Fig. 5 is a diagram of the time evolution of the shock fronts (dashed lines) and contact surfaces (solid lines) when a plasma is first created in the centre of the vessel ($R = 0$) and is later compressed by the imploding shock waves launched from the periphery of the spherical vessel ($R = R$). We observe the following sequence of operations: ⁽²⁾

1. A central plasma is formed, as hot as possible. This plasma is necessarily a rarefied plasma, i.e., of density lower than the original density of the gas in which it is formed;
2. The imploding shock waves collide with this central plasma and start compressing it;
3. During compression, the central plasma temperature increases and significant nuclear reactions begin to take place;

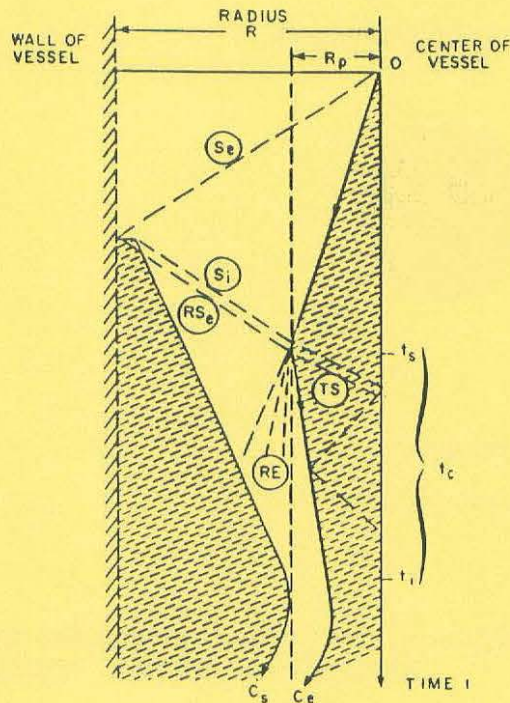


Fig. 5 - Time evolution of spherical pinch operations

4. The reaction rates increase as the central plasma is being compressed;
5. Finally, when the central plasma pressure equals the pressure of the imploding shock waves, equilibrium is reached, and the plasma begins to be disassembled. The phenomenon ends at this time.

SCALING LAW FOR SPHERICAL PINCH EXPERIMENTS

The Spherical Pinch phenomenon is governed by well-known fluid dynamics and shock wave equations. In order to derive the scaling law for breakeven fusion conditions we assume that the reaction rates in the central plasma begin to be significant, during the compression phase, when $T = 2.58$ KeV. From this time on and until the plasma is disassembled we want the plasma to obey the Lawson criterion for breakeven conditions in terms of plasma density and containment time. In planar geometry, the scaling law is:^(2,3)

$$\rho R \left(\frac{E_s}{M_s} \right)^{\frac{1}{2}} \geq 1.96 \times 10^2 \quad \text{cm}^2 \quad \frac{1}{g_2} \quad \frac{1}{J_2} \quad (7)$$

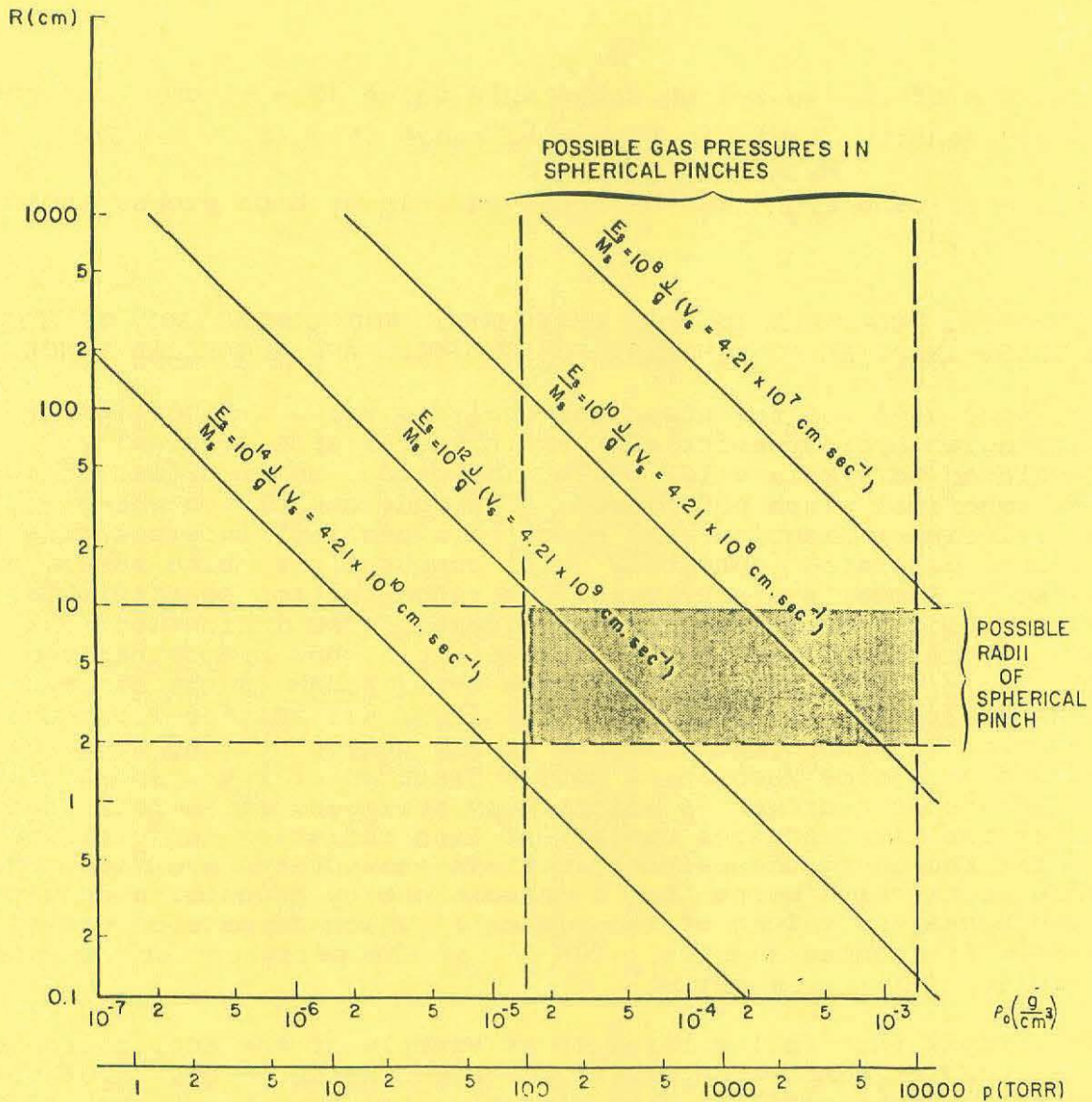


Fig. 6 - Plot of the scaling law for spherical pinch experiments

where:

- ρ is the initial gas density, which is a controllable parameter;
- R is the radius of the vessel, which is a controllable parameter; and
- $\frac{E_s}{M_s}$ is the energy density deposited at the periphery of the vessel, which is a controllable parameter.

If we plot Eq. (7) (Fig. 6), we see that, in order to keep the

radius R of the vessel to acceptable value (2 - 10 cm), and the energy density $\frac{E_s}{M_s}$ within realistic range ($5 \times 10^7 - 10^8$ J/g),

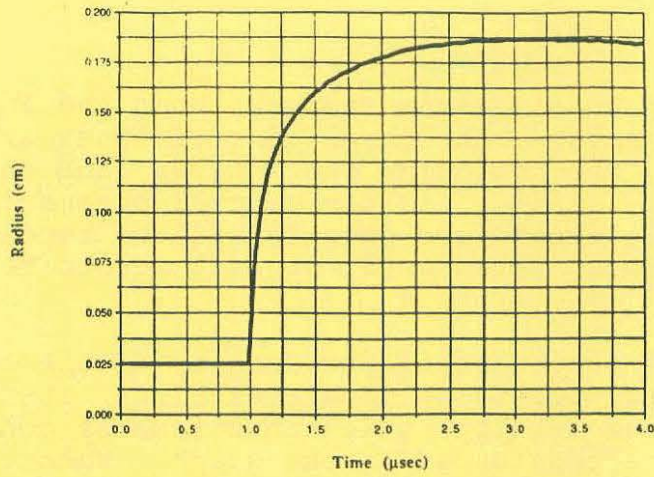
breakeven conditions can be achieved only at high pressures of the working gas.

NUMERICAL ANALYSIS OF THE PHENOMENON AND COMPARISON OF THE TWO MODELS: INERTIAL CONFINEMENT FUSION (ICF) AND SPHERICAL PINCH (SP)

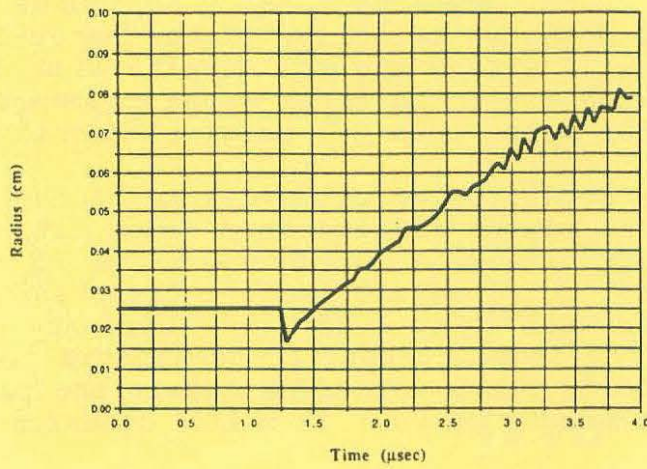
The code used for the numerical analysis was a 1-dimensional, lagrangian hydrodynamics and heat transfer code originally developed to simulate ICF pellet implosion, and modified to model the spherical pinch phenomenon. The code calculates out-of-equilibrium ionization (and electronic density) interpolating from tables generated separately (for computational time sake), and based on Summer's prescription for recombination coefficients, and makes allowance for the cooling effect of the ionization sink. The external wall is treated as adiabatic, but bremsstrahlung cooling of the plasma is accounted for (though in the assumption that the plasma is optically thin, i.e., all emitted light escapes and none is reabsorbed). Since we are only concerned with the plasma at a time when it is hot (a fraction of keV), and at such temperatures hydrogen is essentially stripped, it is felt that under the circumstances neglect of line radiation is justified. As for the energy deposition, certain assumptions are made, the more restrictive being that a certain energy deposition density (and hence the volume of the plasma in which deposition takes place) is assumed a priori: 10^6 J/g at the periphery of the plasma and $\sim 10^7$ J/g at its centre.

The graphs that follow refer to an example of the application of the code for comparison of the ICF with the SP. They refer to: 2 cm radius sphere filled with deuterium-tritium at 100 atm, 43 KJ deposited in 0.5 μ sec at the periphery of the gas in a volume such that the energy deposition density is 10^6 J/g; after 1 μ sec, 43 J are deposited in 0.1 μ sec in the centre of the sphere with an energy deposition density of 6.5×10^7 J/g. For computational purposes, the sphere is divided in 800 concentric spherical shells, the first three in the centre being allocated for the deposition of energy in the central plasma, and the last three at the periphery being allocated for the energy of the imploding shock waves. The graphs refer to the time history of characteristic parameters such as radius, density, etc., of the three central zones.

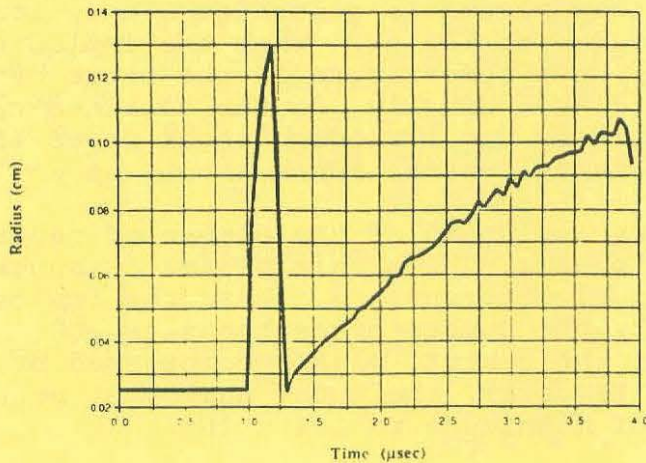
Each figure is composed of three graphs. The upper one refers to the analysis of the time evolution of the parameter of interest when the central discharge acts alone. The central graph refers to the analysis of the time evolution of the parameter of interest when the implosion acts alone. This is clearly the ICF case. The bottom graph refers to the case when both discharges act together. This is clearly the Spherical Pinch case.



Central plasma alone



Implosion alone



Combined central plasma and implosion

Fig. 7 -Time evolution of the radius of the central zones in the case of a) creation of central plasma alone; b) implosion alone, and c) combined central plasma and implosion

Fig. 7 reports the time evolution of the radius of the central plasma. When the central plasma is generated alone, its radius

increases with time, up to a maximum radius. When the implosion is acting alone in the sphere, the three central zones are initially compressed by the imploding shock waves, and then they bounce back and expand. Finally, if the central plasma is generated first, it will expand and then it will be recompressed back by the implosive shock waves until it will return to its original radius.

Fig. 8 reports the time evolution of the density of the central plasma. When the central plasma is generated alone, its density decreases up to a minimum density, which then remains constant for the interval of time considered in the graph. When the implosion is acting alone in the sphere, the three central zones are compressed by a factor of 2.5 by the imploding shock waves, and then they bounce back and the density decreases to values lower than the original density. Finally, if the central plasma is generated first, it will expand and its density will decrease, until such a time when the imploding shock waves recompress it back to a slightly higher value than its original density.

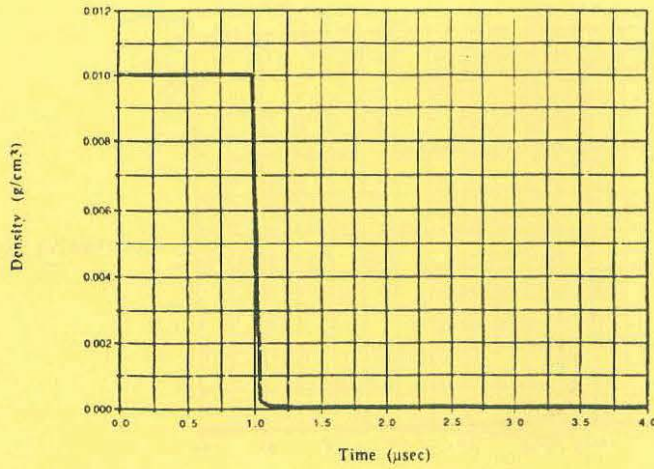
Fig. 9 reports the time evolution of the pressure of the central plasma. When the central plasma is generated alone, its pressure increases up to a maximum of 2.28×10^{10} dynes/cm² (2.25×10^4 Atm). When the implosion is acting alone (ICF case), the pressure in the three central zones increases up to 1.15×10^{12} dynes/cm² (1.13×10^6 Atm). Finally, in the combined case of the central plasma compressed by the imploding shock waves (SP case), the pressure in the three central zones shoots up to 1.67×10^{12} dynes/cm² (1.65×10^6 Atm).

Fig. 10 reports the time evolution of the temperature of the central plasma. When this plasma is generated alone, its temperature reaches a value of 125 eV. When the implosion is acting alone (ICF case), the temperature in the three central zones increases up to 63 eV. Finally, in the combined case of the central plasma compressed by the imploding shock waves (SP case), the temperature in the three central zones shoots up to 205 eV.

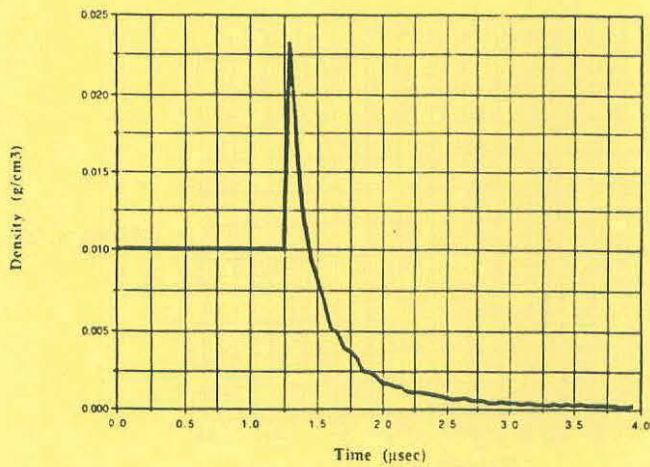
Fig. 11 reports the time evolution of the number of neutrons emitted by the central plasma. When this plasma is generated alone, the total number of neutrons is 3. When the implosion is acting alone (ICF case), the number of neutrons is 200. Finally, in the combined case of the central plasma compressed by the imploding shock waves (SP case), the total number of neutrons increases by 3 orders of magnitude to 1.4×10^5 .

INDUCTIVE SPHERICAL PINCH

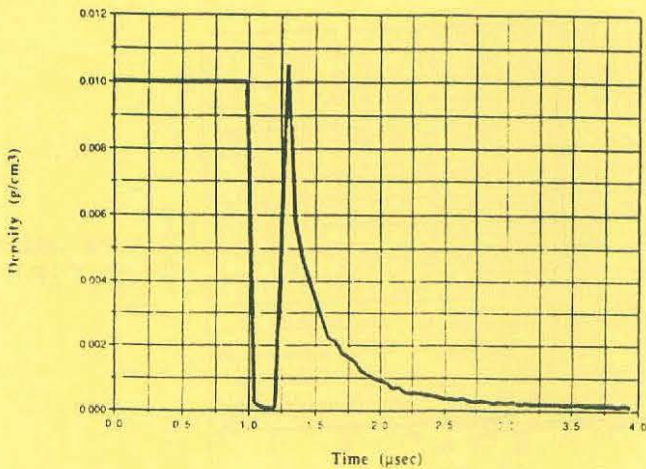
In recent years, the concept of the Spherical Pinch has been exploited for targeted industrial applications. Since the concept has now branched out into two particular directions according to the way energy is deposited into the plasma, namely inductively



Central plasma alone



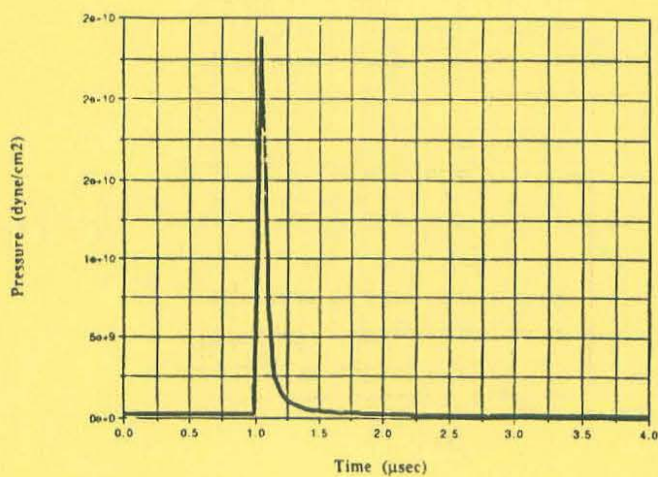
Implosion alone



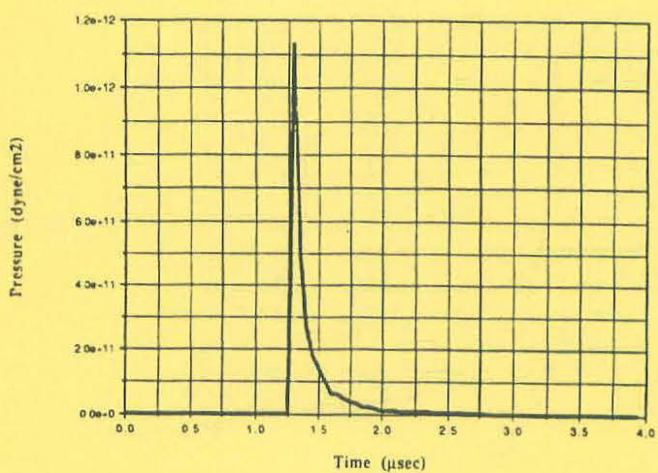
Combined central plasma and implosion

Fig. 8 - Time evolution of the density of the central zones in the case of a) creation of a central plasma alone; b) implosion alone, and c) combined central plasma and implosion.

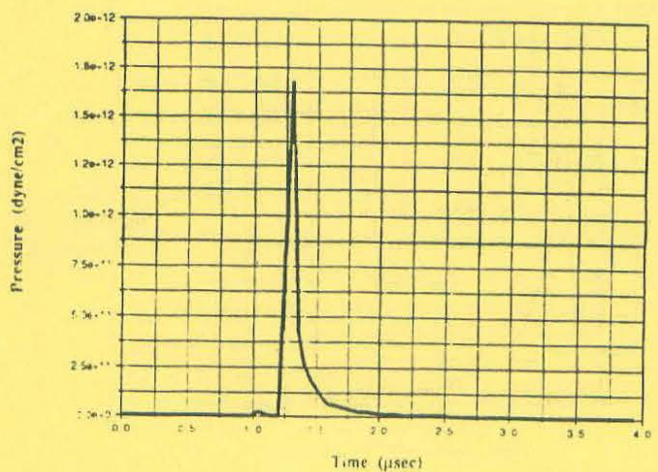
or resistively, we will deal in this section at some length with the inductive pinch and its industrial applications, and will only



Central plasma alone



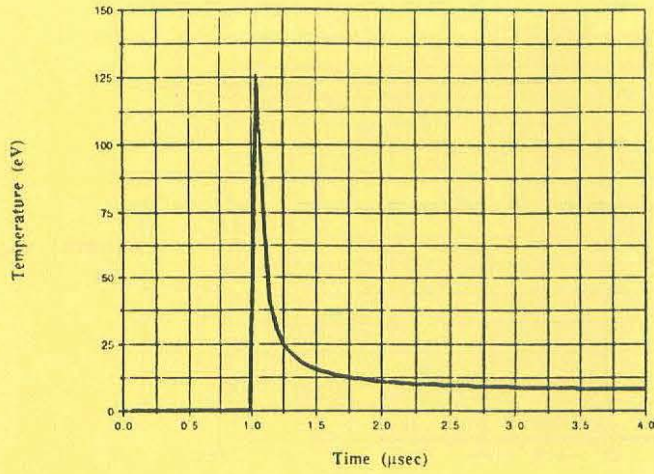
Implosion alone



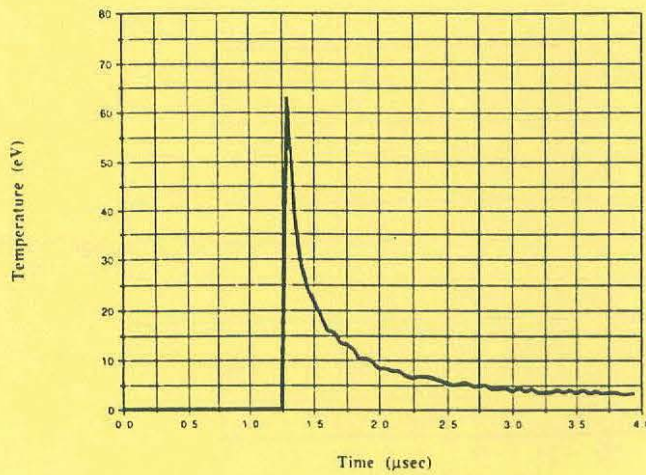
Combined central plasma and implosion

Fig. 9 - Time evolution of the pressure of the central zones in the case of a) creation of a central plasma alone; b) implosion alone, and c) combined central plasma and implosion.

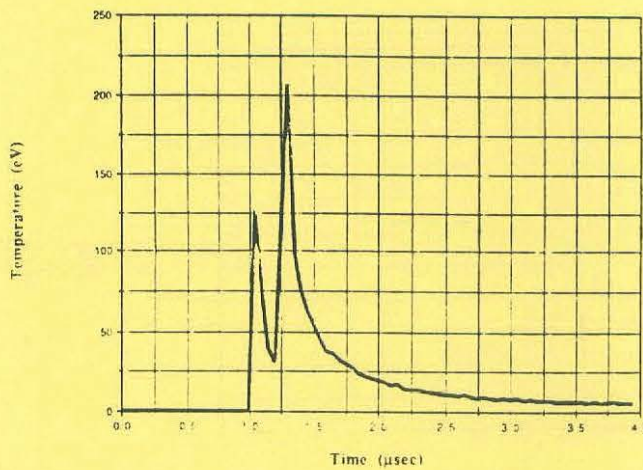
briefly summarize in the next section some of the characteristic features of the resistive pinch.



Central plasma alone



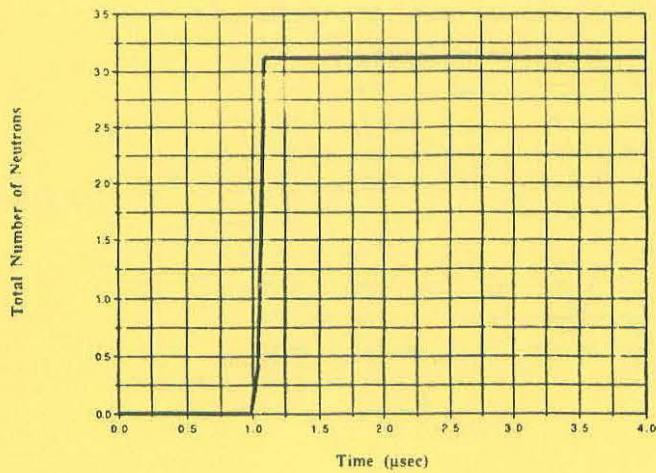
Implosion alone



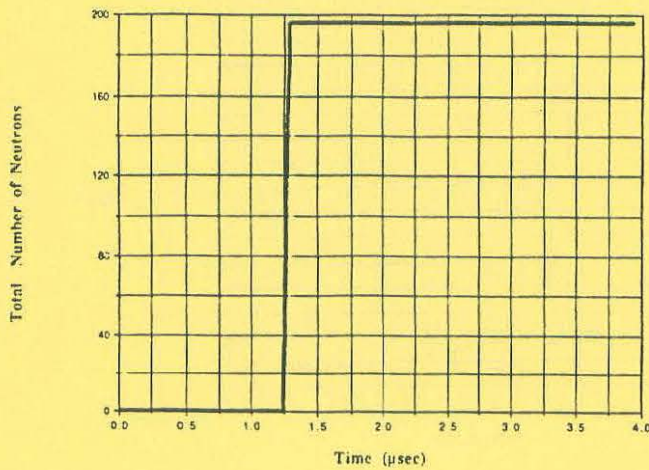
Combined central plasma and implosion

Fig. 10 - Time evolution of the temperature of the central zones in the case a) creation of a central plasma alone; b) implosion alone, and c) combined central plasma and implosion.

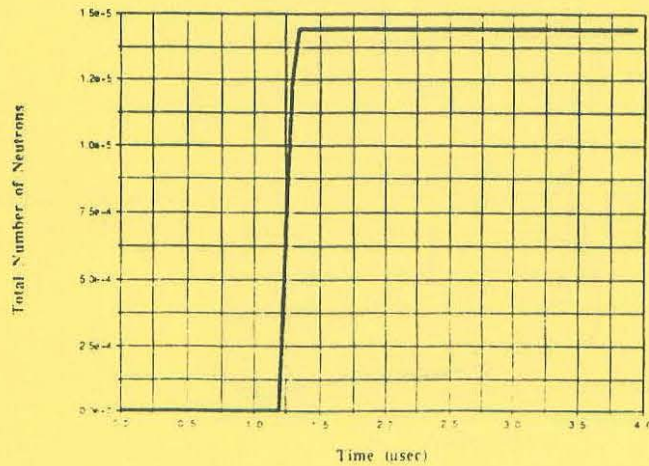
Fig. 12 reports a schematic drawing of the inductive spherical pinch. It is a metallic sphere where slots have been cut in order



Central plasma alone



Implosion alone



Combined central plasma and implosion

Fig. 11 - Time evolution of the total number of neutrons emitted by the central zones in case of a) creation of central plasma alone; b) implosion alone, and c) combined central plasma and implosion.

to direct the current first from the equatorial plane (plane xy) to the north pole, then to the south pole, and then back to

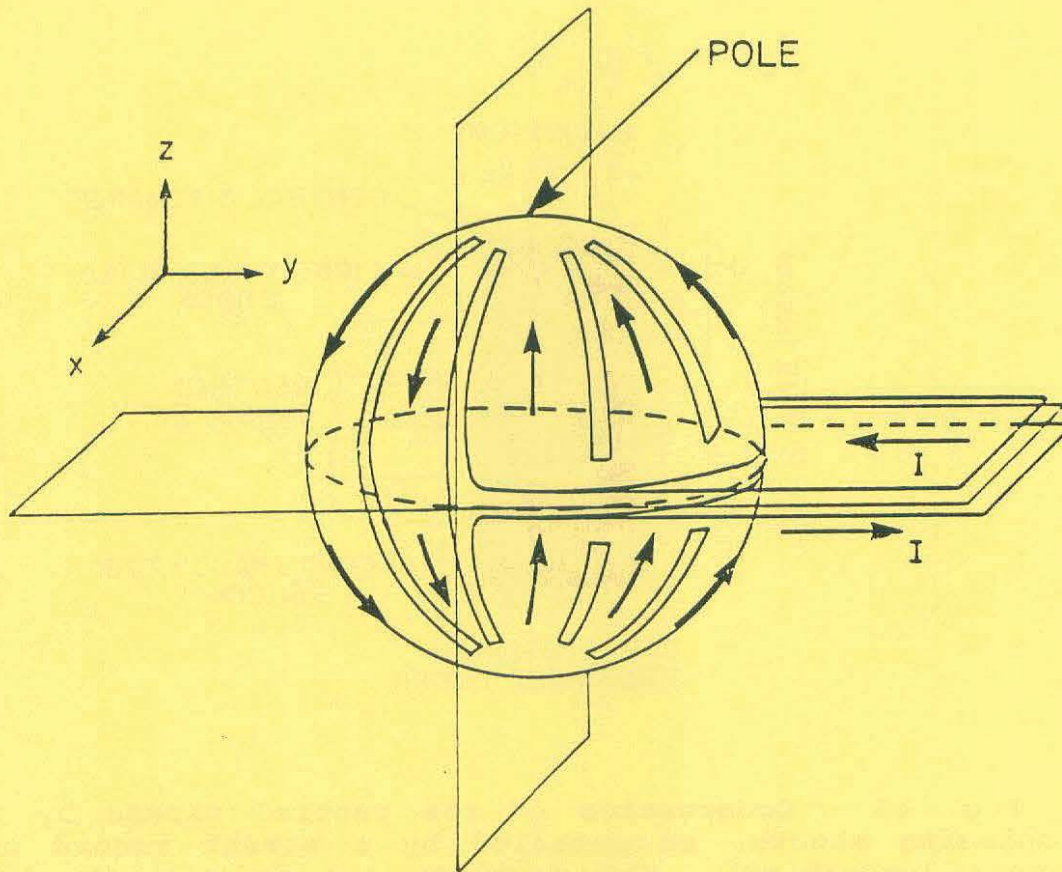


Fig. 12 - Inductive Spherical Pinch

ground in the equatorial plane. A suitable ceramic vessel containing a gas is located within the metallic sphere. Plasmas created in spherical pinches have shown to be very hot and to emit soft X-rays and neutrons.^(1,3,4) Fig 13 shows a streak photograph of the luminosity from the central plasma when this is compressed by the imploding shocks. The record shows that there are two phases of compression caused by the imploding shocks created at every half-cycle oscillation of the condenser bank. The imploding shock trajectories, from the moment they leave the periphery of the vessel until collision with the central plasma, are not recorded on the photograph because they are very strong and hot and, therefore, do not emit much visible radiation, which is the only radiation that the photocathode of the image converter camera can record. However, the shocks transmitted into the central plasma appear clearly and show that their strength decreases from the first compression phase to the second.

The neutron yield from these plasmas can be as high as 3.38×10^8 /discharge in DD and the ion temperature can reach 1.3 keV⁽³⁾.

INDUSTRIAL APPLICATIONS OF THE INDUCTIVE SPHERICAL PINCH

The inductive Spherical Pinch has been utilized for a prototype X-ray generator in order to demonstrate the engineering feasibility

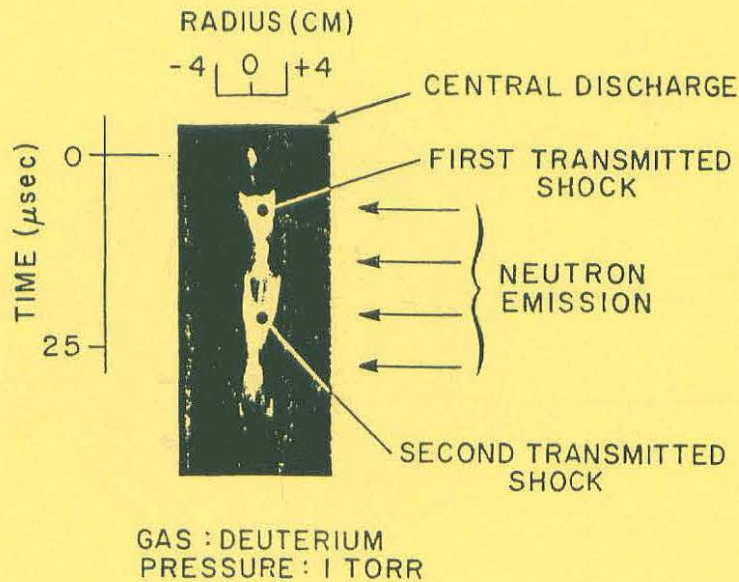


Fig. 13 - Compression of the central plasma by the imploding shocks, as revealed by a streak record of the plasma luminosity. The neutrons are emitted at the time of collapse of the shocks transmitted into the central plasma and at time of maximum plasma compression

of the approach. Design goals of the Spherical Pinch X-ray generator (SPX II) have been:⁽⁶⁾

- high X-ray flux in ~1 keV range
- high energy transfer efficiency
- high repetition rate
- ease of operation
- low electromagnetic noise
- operational flexibility.

Krypton gas is used for optimum X-ray radiation in this preferred spectrum range. Other types of gas such as Argon can be used for different requirements. The gas is automatically filled to a specified pressure (typically 1 Torr) and renewed for each discharge. The energy is stored in a capacitor bank (15 kJ of stored energy at 20 kV charging voltage), then discharged in a low inductance circuit through spark-gap switches. About 20% of the stored energy is deposited into the plasma. A fraction of this absorbed energy is then converted into X-ray radiation. 50 J of X-ray radiation are expected to be emitted from each discharge, which is equivalent to an X-ray flux of 10 mJ/cm² at a distance of 20 cm from the source.

Since X-rays are produced in a pulse of a few microseconds duration, the machine is designed to perform multiple discharges

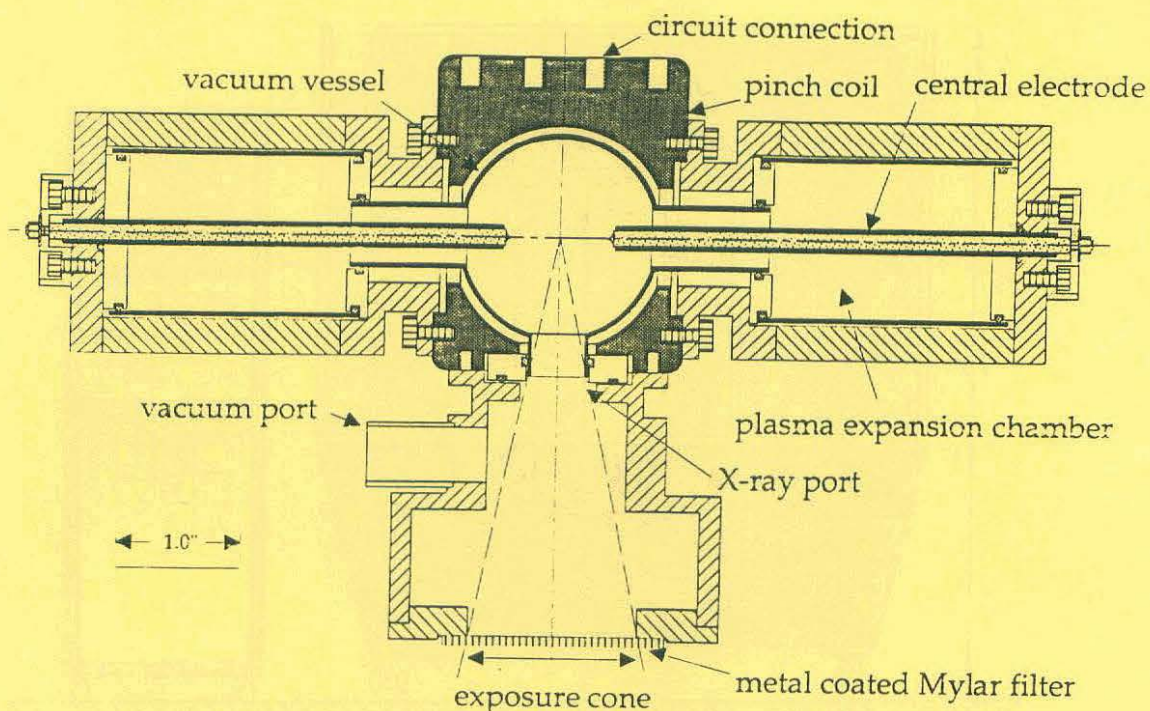


Fig. 14 - SPX II spherical pinch design showing its pinch coil and X-ray port.

up to a number of pre-specified cycles. The repetition rate is currently $\sim 1/10$ Hz (to be increased to $1/5$ Hz) and limited only by the capacity of the high voltage power supply. The machine can be operated fully manually or automatically. In the automatic mode, one needs only to enter a desired number of discharges and then to initiate. The manual operation is for machine optimization or diagnosis.

A schematic of the spherical pinch coil and X-ray port is given in Fig. 14. The X-ray port is oriented vertically under the pinch as shown. A metal coated Mylar window of 0.001" thickness is used to isolate the discharge gas and to maintain the proper pressure in the discharge vessel. Another port will be added to monitor the X-ray flux from each discharge and to integrate it to control the total dosage over multiple discharges. Fig. 15 shows the overall dimensions of the prototype which consists of a discharge unit and a control console.

Table I reports the technical characteristics of the SPX II machines. Table II reports the flux per discharge in mJ/cm^2 at 20 cm from the radiation source transmitted through suitable filters.

Finally, Table III shows the parameters of the commercial machine SPX III which is now being built. This is a commercial machine,

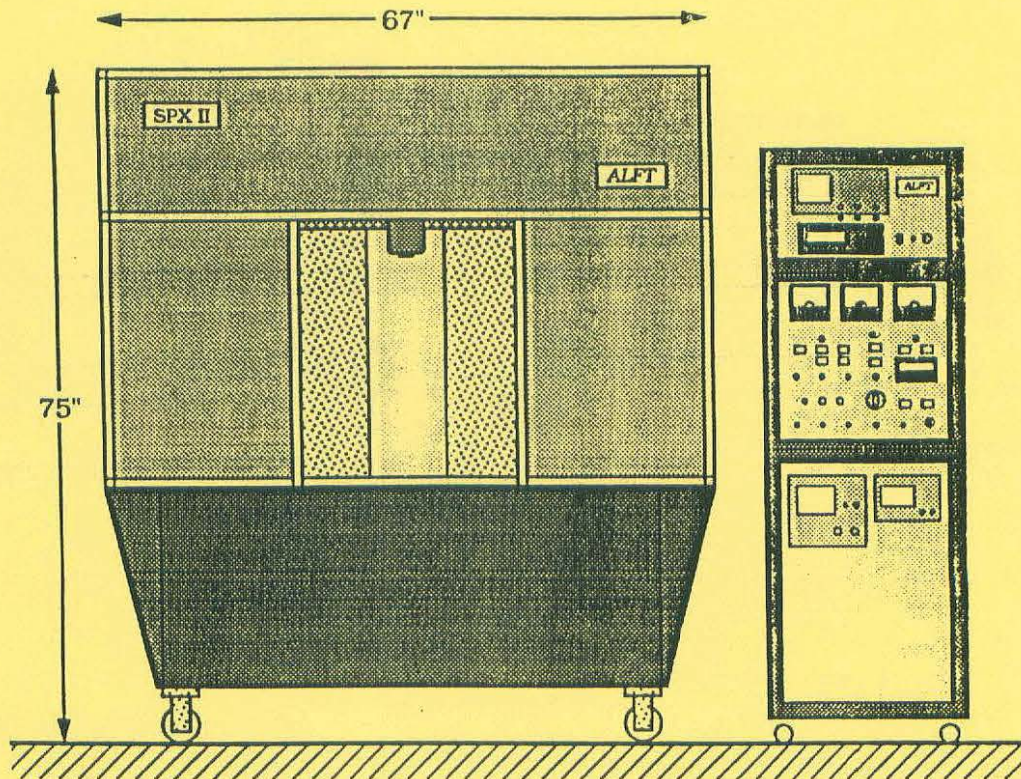


Fig. 15 - SPX II prototype X-ray generator, overall configuration.

designed to satisfy more closely the requirements of the microlithography industry. The parameters of the SPX III machine are compared with those of the SPX II machine in the same Table.

RESISTIVE SPHERICAL PINCH

For fusion purposes, the scaling law for breakeven conditions of Eq. (7) (see Fig. 6) indicates that a gas pressure of several hundred atmospheres is required in order to keep the radius of the vessel within reasonable limits (2-10 cm). At these pressures, energy deposition into the gas by inductive means is not possible. An alternative method is therefore adopted, the resistive method, whereby the deposition of energy at the periphery of the spherical vessel takes place, as with the central plasma, through sparks, although, of course, any other suitable means of energy deposition is equally valid.

In a pilot experiment, the configuration that we adopted was to create a multitude of peripheral sparks replacing the inductive discharge.⁽⁴⁾ Each spark was fed by individual condensers of 0.5 μ F, charged to ~10.5 KV. Moreover, since it was important in this

Parameters	Units	SPX II
Operating Voltage (max)	kV	30
Stored energy	kJ	34
Energy transfer to plasma	%	20
Peak current	kA	1200
Repetition rate	Hz	0.1
Gas pressure	Torr	1
Gas Volume	ml	250
X-ray output/pulse (max)	mJ/cm ²	10
Distance from source	cm	20
Pulse duration	μsec	>1

Table I - Technical characteristics of the SPX II machine.

Radiation (Å)	Soft X-ray 10 - 15	XUV 50 - 150	Deep UV 600 - 1800	UV 1800 - 3500
Rad. Flux (mJ/cm ²)	1 - 4	400	91	150

Table II - Flux per discharge in mJ/cm² at 20 cm from the radiation source through suitable filters.

pilot experiment to be able to visualize the plasma motion, we adopted a cylindrical configuration, rather than spherical. In other words, the vessel was a cylinder of 1.15 cm height and 2 cm radius, closed on one side with a metal plate and open on the other side, from where the plasma can be observed. Thirty six electrodes were radially accommodated along the peripheral circle of the cylinder so as to have 36 sparks. In the centre of the vessel another spark is created by discharging between two electrodes a 0.5 μF condenser charged to 10.5 KV. By carefully adjusting the gap of the central spark, self-breakdown of this gap occurs first, the UV radiation from the plasma so created

Parameters	Units	SPX II	SPX III
Operating Voltage (max)	kV	30	30
Stored energy	kJ	34	60
Energy transfer to plasma	%	20	25
Peak current	kA	1200	1500
Repetition rate	Hz	0.1	1
Gas pressure	Torr	1	1
Gas Volume	ml	250	50
X-ray output/pulse (max)	mJ/cm ²	10	12
Distance from source	cm	20	30
Pulse duration	μsec	>1	>5

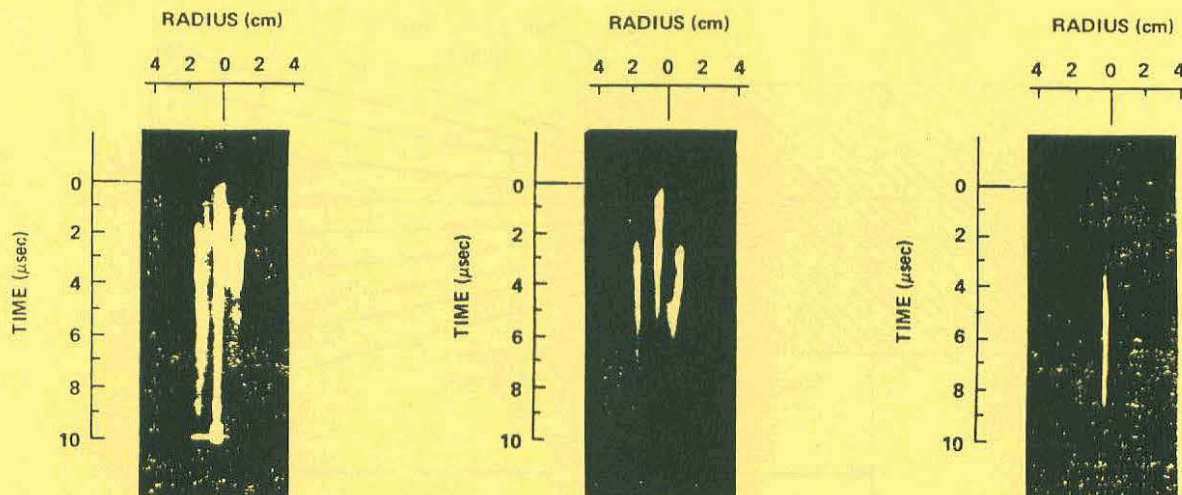
Table III - Parameters of the commercial machine SPX III.

triggering all peripheral discharges. The cylindrical vessel, as described, is located in a high-pressure chamber provided with a window, from which the plasma evolution can be observed.

Figure 16 shows three streak records of the central plasma when it is compressed by the imploding shocks. The first record at the left is essentially a record of the plasma luminosity time history, as observed with an image converter camera through a narrow slit oriented along a diameter of the cylindrical discharge chamber. The original pressure of hydrogen gas in the chamber was 8 atm = 6,000 Torr, corresponding to a density of $2.14 \times 10^{20} \text{ cm}^{-3}$. The condenser bank energy used for the implosion was ~1 KJ, whereas for the central discharge the energy was ~30 J. This record shows that the central plasma is being compressed by the imploding shocks, but not much information beyond this is available.

Since the plasma luminosity can only provide a general indication of the events occurring in a plasma, we reduced the recorded plasma luminosity by decreasing the width of the slit in front of the camera and obtained the streak record shown in the middle of Fig. 16. We observe now that the central plasma seems to disappear at $t \approx 6 \mu\text{sec}$ from the initiation of the discharge. In other words, the plasma becomes black at the time when maximum compression begins to take place. Clearly, this effect is a manifestation that the plasma blackbody radiation, because of the compression and subsequent temperature rise, shifts toward the XUV range.

In order to have a confirmation of this we placed in front of the camera a narrow band interference filter centered at $\lambda = 3,900 \text{ \AA}$ and having bandwidth 60 \AA . We virtually rejected in this way all visible light and let only light at 3,900 \AA cross the slit (whose



GAS: HYDROGEN
PRESSURE: 116 psi = 8 Atm = 6000 Torr
DENSITY: $2.14 \times 10^{20} \text{ cm}^{-3}$
CONDENSER BANK ENERGY:
PERIPHERAL DISCHARGES ~ 1kJ
CENTRAL DISCHARGE ~ 30J

Fig. 16 - Streak records of the central plasma, when this is compressed by the imploding shocks. The record at left is the time history of the plasma luminosity. The centre record is the time history of the plasma when its luminosity has been greatly reduced. The record at the right is the plasma as observed through a narrow-band interference filter centered at $\lambda = 3,900 \text{ \AA}$ and bandwidth 60 \AA . This is the hottest plasma, which is stable and lasts 5.4 μsec . All discharges are in hydrogen at 6,000 Torr initial pressure.

width was slightly increased for this purpose), thus reaching the image converter camera. The streak record at the right of Fig. 15 shows the plasma as it appears through the narrow band filter. Clearly, this is the hottest plasma formed during the compression phase of the central plasma. This remarkably stable plasma begins to appear at about 3.5 μsec after the initiation of the discharge and lasts for 5.4 μsec .

The same experiment was then repeated by fully enclosing the cylindrical discharge chamber with a metal plate working with deuterium, rather than hydrogen gas. Four calibrated silver activation neutron detectors were radially and symmetrically placed in a 60° solid cone angle having apex at the central plasma. Neutrons were detected in this experiment. Within the

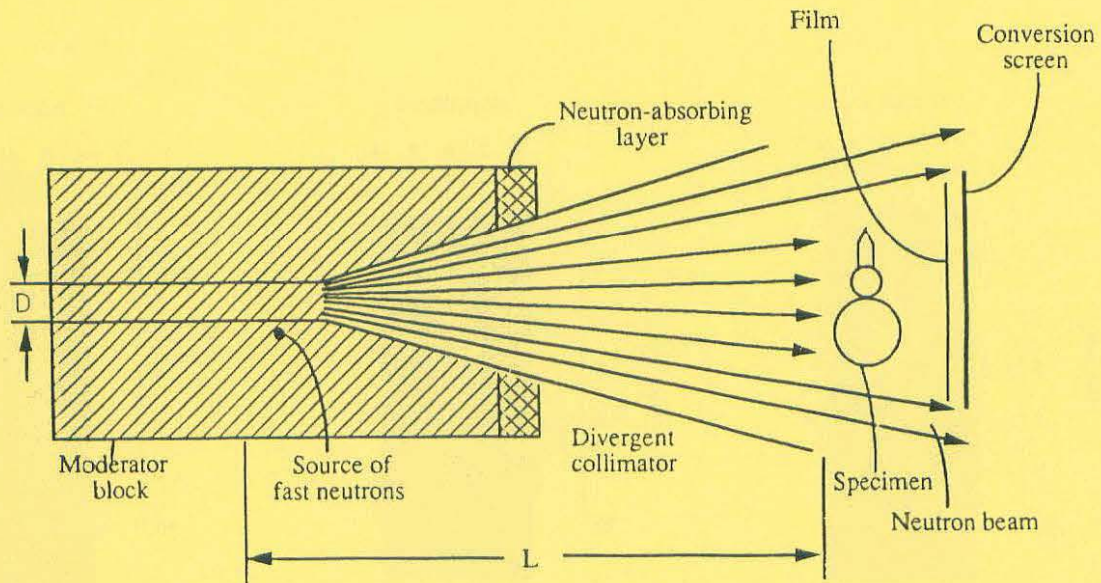


Fig. 17 - A flux of 10^6 neutrons/cm² are required at the position of the sample (~40 cm from the neutron source) for a total number of 10^{10} neutrons/discharge emitted by the source.

above solid angle, and within the experimental errors, the neutrons were symmetrically emitted. Their average number was 7.11×10^6 per shot.

INDUSTRIAL APPLICATIONS OF THE RESISTIVE SPHERICAL PINCH

One of the first possible industrial applications of the resistive Spherical Pinch is in neutron radiography for non-destructive testing of materials. Fig. 17 shows in schematic form the principle of neutron radiography. A proof-of-principle experiment of neutron generation with the Spherical Pinch will be shortly conducted with a 1 MJ condenser bank facility located in the NRC campus in Ottawa and the details will be provided in a successive publication.

CONCLUSIONS

The Spherical Pinch concept of plasma heating offers several advantages relative to other known fusion concepts, the most notable being that its scaling law for breakeven conditions is known and understood. This allows an experimental approach to fusion through modest scale experiments, rather than expensive ones. Moreover, the Spherical Pinch is providing immediate industrial applications, such as X-ray generation for microlithography, which are not possible with other more expensive approaches to fusion.

For these reasons, the Spherical Pinch is gaining acceptance among

the international plasma and fusion physics community, and several groups are now working on this concept, such as the Department of Physics of the University of Miami, the Institute of Atomic and Molecular Physics of the National Research Council of Italy in Pisa, the Department of Mathematics of the University of Texas, etc. It is believed that Canada should direct a portion of its national fusion effort along the line of research of the Spherical Pinch in order to maximize the chances of success in the fusion race and to acquire a leadership position in the world.

ACKNOWLEDGMENT

This work has been possible thanks to the collective effort of many people. In particular, thanks must go to S. Aithal, V. Guty, B. Hilko, K. Kawai, M. Lamari, D. Mostacci, and P. Savic.

REFERENCES

1. E. Panarella, *Can. J. Phys.* 58, 983 (1980).
2. E. Panarella, and P. Savic, *J. Fusion Energy* 3, 199 (1983).
3. E. Panarella, and V. Guty, *Proc. 1982 IEEE Intern. Conf. on Plasma Science, Ottawa, Canada, 17-19 May 1982*, p. 135.
4. E. Panarella, *J. Fusion Energy* 6, 285 (1987).
5. P. Savic and E. Panarella, *J. Appl. Phys.* 59, 3990 (1986).
6. K. Kawai, E. Panarella, and D. Mostacci, *SPIE Proc. Vol. 1465 (1991)*, p. 308; S. Aithal, K. Kawai, M. Lamari, and E. Panarella, *SPIE Proc.*, Vol. 1671 (1992).
7. D. Mostacci, K. Kawai, E. Panarella, and N. Salingaros, *Bull. Amer. Phys. Soc.* 35, 1963 (1990).
8. J. D. Lawson, *Proc. Phys. Soc. B*, 70, 6 (1957)
9. J. P. Somon, in "Physics of High Energy Density" (Academic Press, New York 1971), Eds. P. Caldirola and H. Knoepfel, p. 189.
10. B. Ahlborn and M. H. Key, *Plasma Physics* 23, 435 (1981).